50mm Diameter Sn-doped (001) β-Ga_2O_3 Crystal Growth using the Vertical Bridgeman Technique in Ambient Air

*K. Hoshikawa[1,2], T. Kobayashi[1], E. Ohba[2], T. Kobayashi[2]
Faculty of Engineering, Shinshu University, Nagano, Japan[1]
Fujikoshi Machinery Corp., Nagano, Japan[2]
*E-mail: khoshi1@shinshu-u.ac.jp

Abstract

50 mm-diameter Sn-doped β-Ga_2O_3 crystals with growth orientation perpendicular to (001) plane were grown with the newly-developed resistance heating vertical Bridgeman furnace using platinum-rhodium alloy crucibles in ambient air. Weak low angle grain boundaries and several small grains were detected on the both-side mirror-polished 50 mm-diameter (001) wafer, using high resolution refraction x-ray topography. However, no imperfections were observed over the whole wafer area when using crossed polarizer analysis. Measured values of both the full width at half maximum and the dislocation densities were widely distributed in the wafer, ranging from 10 to 50 arcsec and 100 to 2000 /cm^2 respectively with no distinctive correlations among them. The Sn-doped crystals with concentrations ranging from 5 x 10^{17} to 5 x 10^{18} atom/cm^3 could be grown by Sn-doping in a range from 0.05 to 0.1mol%, and (001) oriented, 50 mm-diameter n-type oxide semiconductor wafers with a carrier density of 3.6 x 10^{18} /cm^3, a mobility of 60 cm^2/Vsec and a resistivity of 0.03 Ω-cm, were obtained from a 0.1mol% Sn-doped crystal.

Key words;
A1. X-ray topograph
A1. Doping
A2. Bridgman technique
A2. Single crystal growth
B1. Oxides
B2. Semiconducting β-Ga_2O_3

1. Introduction

β-Ga_2O_3 is an oxide semiconductor with a wide band gap of 4.7-4.9 eV [1, 2]. It has recently been attracting attention as a material for next-generation power devices featuring high power, high breakdown voltage and high current density [3-5]. Research into growth techniques that produce larger and better quality β-Ga_2O_3 crystals has intensified recently [6, 7]. β-Ga_2O_3 bulk crystals have until now been grown by optical floating-zone (OFZ) [8-10], Czochralski (CZ) [11-13] and edge-defined, film-fed growth (EFG) [6, 14] methods. β-Ga_2O_3 substrates grown by the EFG method have recently become commercially available [15].

Both CZ and EFG techniques are widely known as methods suitable for producing large size and high-quality crystals. However, β-Ga_2O_3 crystal growth by CZ or EFG techniques in which iridium crucibles or iridium crucibles and dies are used presents some technical problems relating to atmosphere control that it is essential to solve. An oxidizing atmosphere is desirable for β-Ga_2O_3 crystal growth because it is an oxide that undergoes reductive decomposition ($Ga_2O_3 \rightarrow 2Ga + 3/2O_2$) at high temperatures due to a deficiency of oxygen [11-13, 16, 17]. This problem links to the fact that iridium crucibles are not useful in atmospheres with more than a few percent of oxygen partial pressure at the high temperature required to melt β-Ga_2O_3, because iridium will easily oxidize and evaporate under those conditions [13, 18]. These considerations indicate that the suppression of both iridium oxidization and Ga_2O_3 decomposition are in conflict, due to the need for high temperature during the growth of β-Ga_2O_3 in both CZ and EFG methods.

To solve this problem, we have proposed a new approach in which β-Ga_2O_3 crystals are grown in ambient air, as suppressing Ga_2O_3 decomposition is the most important issue for the growth of larger and better quality β-Ga_2O_3 crystals. We have studied the growth of single crystals of β-Ga_2O_3 by the vertical Bridgman (VB) method, in which diameter control was unnecessary and the crystals could be grown in a very low temperature gradient [19-21]. As a result of these conditions, we were able to use platinum-rhodium alloy crucibles, the melting temperature of which is approximately 50°C higher than the melting temperature (1793°C) of β-Ga_2O_3 [22], and the crucibles with better resistance to oxidation were also useful in the oxidizing atmosphere, including ambient air, in which an iridium crucible is far from adequate.

We reported in our previous papers [22, 23] the successful growth of single crystals of β-Ga_2O_3 about 25 mm in diameter, by the VB method, using platinum-rhodium alloy crucibles in ambient air. In our early VB furnace [22], however, we had used a radio

frequency heating technique to realize high temperatures inside the VB furnace. However, following several years of study, we came to the conclusion that a VB furnace with more uniform temperature distribution in the large furnace zone had to be developed if we were to succeed in growing larger size and better quality β-Ga_2O_3 crystals. To solve this, we have worked to construct a resistance heating furnace with molybdenum silicide heaters, and ultimately developed a VB furnace which can achieve temperatures above 1830°C in ambient air. More recently, using this furnace, we have successfully grown 50mm-diameter single crystals of β-Ga_2O_3 with growth orientation perpendicular to (100) plane, and confirmed that the total weight loss during a VB growth run is very small, amounting to less than 1% of the total weight of the platinum-rhodium alloy crucible and the Ga_2O_3 raw material [24].

In this paper, by using the developed VB furnace, we will study the growth of 50mm-diameter Sn-doped single crystals of β-Ga_2O_3 with growth orientation perpendicular to (001) plane, which have been widely used for epitaxial substrates [25, 26]. We will present the features of as-grown crystal ingots produced by the VB technique, the characteristics of crystallinity of 50 mm-diameter (001) wafers machined from the ingots, and the electrical properties of Sn-doped wafers, along with an impurity analysis.

2. Experimental

50 mm-diameter Sn-doped (001) β-Ga_2O_3 crystals were grown in a resistance heating VB furnace [24] using platinum-rhodium alloy crucibles in ambient air [22-24]. The resistance heating VB furnace which we have newly developed is described in detail in our previous papers [24]. In the present experiment, 5N Ga_2O_3 raw material powder was mixed with 0.05 to 0.5mol% 4N SnO_2 powder in a 24-hour ball-mill process and the mixture was sintered at 1500°C for 5 hours in ambient air after a cold isostatic pressure shaping process. A seed crystal was shaped with a cross section of 3.5 x 3.5 mm^2 and a length of 30 mm with (001) growth direction and it was mounted in the thin seed well, which had a 5 mm inner diameter, of the platinum-rhodium alloy crucible.

The VB crystal growth processes were virtually the same as those reported in our previous paper [24]. The crucible, charged with a seed crystal and a sintered body of Ga_2O_3 raw material, was elevated to the high temperature zone in order to ensure the melting of all the raw material and also some part of the seed crystal during the seeding process. Then the crucible was lowered at a translation rate of 1.0 to 2.0 mm/hour during the VB growth process. The crucible was rotated at a constant rate of 3 to 5rpm during

seeding and growth processes. The crystal grown by the VB process in the platinum-rhodium alloy crucible was released from the crucible by destructively peeling it from the crystal periphery [22]. The crystal ingot was annealed at 1500^{o}C for 10 hours in ambient air to remove residual thermal stress remaining from the growth process.

(001) wafers of about 1 mm thickness were sliced from the crystal ingot with an inner blade slicer and both sides underwent lapping and polishing to produce a stress-free mirror surface. Refraction x-ray topography was conducted using a high resolution (5.4μm/pixel) Rigaku XRTmicron with Cu Kα radiation on $\boldsymbol{g_{605}}$ or $\boldsymbol{g_{2\text{-}25}}$ for the whole (001) plane. X-ray rocking curve analysis was also conducted with the Rigaku XRTmicron with (2-24) diffraction by an Si (440) double crystal monochromator, and full width at half maximum (FWHM) measurement carried out on five portions of 5 x 9 mm^2 area with a low x-ray incidence angle of about 9 degrees and the resolution is estimated as 0.7 arcsec. Etch pits formed after KOH solution etching on the mirror-polished (001) plane were observed by the differential interference contrast microscopy. The impurity analysis was conducted by GDMS using VG Elemental VG9000 for ten elements of expected dopant Sn, Pt and Rh contamination from crucible materials and other elements during the growth processes. The Hall effect measurement was conducted by the Van der Pauw method using Toyo-technica ResiTest type8330 for 5 x 5 mm^2 samples with Ti-Au electrodes at a room temperature of 22^{o}C.

3. Results and discussion

3.1 Features of as-grown crystal ingots by VB technique

Figure 1 presents photographs of as-grown 50 mm-diameter Sn-doped β-Ga_2O_3 crystals with growth orientation perpendicular to (001) plane. In Fig.1(a), the upper sections of each crystal are seed portions still attached to the seed wells of the platinum-rhodium alloy crucibles. The crystals A and B in Fig. 1(a) are turned upside down from their orientations during their growth processes and each crystal surface in Fig. 1(b) is the end portion of the growth. The growth end portion of most crystals have a visual appearance similar to crystal A in Fig. 1(b). Sometimes, however, we can grow complete single crystals in our VB growth of (001) β-Ga_2O_3 crystals, as crystal B in Fig. 1(b) demonstrates. As 100% solidification of melt in the crucible is essential in the VB growth process, the solidification of a complete single crystal right up to the growth end portion has generally been very difficult. This is because a breakout - meaning a growth transition from a single

crystal to polycrystal - often occurs due to factors such as a composition shift, an impurity accumulation and others, in addition to inadequate thermal conditions near the growth interface. However, it was found in the present VB β-Ga_2O_3 growth that the polycrystal portions by the breakout in the final several percent of residual melt were formed only at the thin surface and periphery regions of the growth end portions and that these polycrystal portions did not affect the generation of cracks and/or cleavages in the single crystal body either during the cooling process of crystal ingot after growth or during the machining process from ingot to wafers. We concluded in our present study that the breakout at the growth end portion is not so serious a problem in the crystal growth and wafer processes as for β-Ga_2O_3 crystals with growth orientation perpendicular to (001) plane.

We also found that another feature of the growth end portion surface of the complete single crystal was that it was smooth and shining as shown in crystal B in Fig. 1(b), while a needle-shaped surface morphology aligned parallel to the crystallographic [010] direction was observed at the end portion surface of the breakout crystal A in Fig. 1(b). The surface morphology with the [010] lines may be similar to that formed by the needle-like crystal growth documented in our previous paper [22]. The differences in growth features between crystals A and B in Fig. 1 are hard to clarify at present and further investigation into them will be one of our future research subjects. The slight difference in crystal color between crystals A and B in Fig. 1 might be a result of the different Sn-doping levels used for crystals A and B, which were 0.05 and 0.1 mol% respectively. The color of the as-grown crystal body gradually changed from dark yellow to dark green as the Sn-doping level was increased.

3.2 Characteristics of crystallinity on 50 mm-diameter (001) wafers

Figure 2 is a photograph of 50 mm-diameter both-side mirror-polished (001) β-Ga_2O_3 wafers with about 0.7 mm thickness. The slicing and polishing of (001) wafers were rather easier than that of (100) wafers [24]. This is because (001) cleavage in the slicing process and micro-cracks and micro-cleavage on the (001) plane in the lapping and polishing processes were not found as in the case of the (100) plane [24]. However, as we are not at present able to machine a well beveled mirror periphery, numerous micro cleavages with (100) plane nearly perpendicular to the (001) wafer plane, were formed along the whole wafer periphery during the slicing, lapping and polishing processes. The micro cleaving occurs on the (100) plane parallel to the [010] crystallographic direction and often results in wafer separation. And these make the successful production of mirror-

polished wafers very difficult. Consequently, we have concluded for the moment that the small notch geometry with (100) cleavage plane at [100] periphery of (001) wafers indicated by the arrows in Fig. 2 is difficult to eliminate, and may in any case be useful as an orientation flat.

Figure 3 shows a crossed polarizer observation image (Fig. 3(a)) and a refraction x-ray topographic image (Fig. 3(b)) of 50 mm-diameter (001) wafers that were obtained from the crystal ingot A shown in Fig. 1 after our available quality machining processes. Some weak low-angle grain boundaries (LAGBs) with [010] direction and several small grains at the center portion of the wafer were detected in the refraction x-ray topography in Fig. 3(b). On the other hand, no imperfections were observed across the whole wafer area, except for fringe patterns showing some wafer thickness difference in our crossed polarizer analysis shown in Fig. 3(a). We presume that the LAGBs and the grains observed by the refraction x-ray topography may originate from some imperfections in the seeding process [21, 27].

Figure 4 shows a crossed polarizer observation image (Fig. 4(a)) and a refraction x-ray topographic image (Fig. 4(b)) of 50mm-diameter (001) wafers that were obtained from the crystal ingot B shown in Fig. 1. No imperfections were observed across the whole wafer area in the crossed polarizer image. We might conclude that the crystal ingot B in Fig. 1 had been grown as a complete single crystal due to the visual appearance of the end portion in photograph B in Fig. 1(b) and the crossed polarizer observation in Fig. 4(a). However, several LAGBs and two grains were detected in Fig. 4(b) with high-resolution refraction x-ray topography with the Rigaku XRTmicron. A volume of micro cleavages at the outer wafer periphery was also detected in Fig. 4(b). Our conjecture is that these micro cleavages must be formed due to our machining processes but that the LAGBs and the grains might originate from some processes during crystal growth.

Figure 5 shows x-ray rocking curves on the wafer shown in Fig. 4(b). The curves 1, 2, 3, 4 and 5 correspond to the numbered 5 x 9 mm^2 portions indicated by the rectangles in Fig. 4(b). The curve 6 is a reference rocking curve measured on a dislocation-free (100) silicon sample by using the same x-ray rocking curve analysis. The FWHM values [13, 28] calculated from each curve are indicated respectively in the figures. They are spread over a range from 8.6 arcsec at position 3, to 46.1 arcsec with a double peak rocking curve at position 4. We may perhaps say that the FWHM values of our (001) β-Ga_2O_3 wafer were very small and close to those for a dislocation-free silicon wafer when the better or best quality portions in the wafer were selected randomly as measuring portions.

Figure 6 shows photographs of two kinds of etch pits A and B revealed by KOH solution etching after the x-ray topography analysis shown in Fig. 4(b). Figs. 6(a) and (c)

show etch pits A and B - a large and clear-shaped low density pit and a tiny point-like high density pit - observed in the small area indicated by rectangle 5 in Fig. 4(b). Figs. 6(b) and (d) show etch pits A and B observed in the small area indicated by rectangle 3 in Fig. 4(b). We judged from their shape, distribution and density that the A etch pits were dislocation pits originating in the bulk crystal, and that the B etch pits might be surface defects caused by the wafer machining processes. We found that the dislocation densities shown by the A pits were 98 /cm^2 at minimum in the area indicated by rectangle 2 and 2100 /cm^2 at maximum in the area indicated by rectangle 1, which were relatively smaller values than those reported in our previous paper [23].

The distribution characteristics of the FWHM and densities of etch pits A and B for the five areas on the wafer indicated by rectangles in Fig. 4(b) are summarized in Table 1. We can say then of the characteristics of a representative (001) β-Ga_2O_3 wafer that the FWHM and the densities of etch pits A and B showed random values, while no clear correlations between them were found in this study.

3.3 Impurity analysis and electric properties on Sn-doped crystals

Results of the GDMS impurity analysis on two crystal ingots are shown in Table 2. The analyzed values of crystals A and B in Table 2 are the results for crystals grown with 0.05 and 0.1 mol% mixing of dopant SnO_2 to raw material 1/2Ga_2O_3. The two samples were cut respectively from the cylindrical portion of the grown crystal just beyond the conical portion, with approximately 0.2 solidification fraction (g=0.2). The purity of raw material used was five nines (99.999%), and the concentration of each residual impurity element analyzed was less than 1.0 ppm by weight (wt.ppm), according to the data from Yamanaka Hutech Corp.. We can note as a feature of the results in table 2 that several tens wt.ppm rhodium contaminant came from the platinum-rhodium alloy crucible [22] and the several wt.ppm Si, Fe and Zr might result from contamination by furnace materials [22]. The concentration of dopant Sn increased from 14 to 83 wt.ppm as the doped Sn concentration in the raw material was increased from 0.05 to 0.1mol%. However, no linear relation in the concentration was found between the doping amount and the resulting concentration in the crystal grown. The dopant Sn concentration in the crystals may relate to several contributing factors during the VB crystal growth processes as we will discuss below.

Table 3 shows the relation between the solidification fraction g and Sn concentration for a crystal with 0.1mol% Sn-doping grown with a 2 mm/h crucible translation rate. The Sn concentration in the initial melt, that is the molten Ga_2O_3 just after the melting process, was calculated to be approximately 630 wt.ppm. As a result, we could simply calculate

the segregation coefficient to be approximately 0.27 using an Sn concentration of 170 wt.ppm at g=0.10 when we roughly assumed that Sn concentration of melt at g=0.10 did not differ so much from that of the initial melt at g=0. According to the normal freezing process with segregation coefficient less than unity, the concentration valuation with g increase must be gradually increased and then rapidly increased during the final growth process in the VB manner with 100% solidification. It is clear that the above consideration of Sn segregation is in conflict with the experimental result shown in Table 3 as Sn concentration decreased 170 to 83 wt.ppm corresponding to g=0.1 to 0.2 and did not change within the experimental error in the crystal with g ≥ 0.2. We might attempt to explain the above conflict as being due to doped Sn being easily lost due to evaporation from the sintered body and molten Ga_2O_3, and by separation from them as oxide SnO_2 and/or decomposed species Sn during the melting and growing processes [29]. In this case, the segregation coefficient of Sn might be larger than 0.27 when Sn evaporation loss during the melting and melt stabilizing processes before growth start is taken into account. As a result, we could say that the doping Sn concentration to β-Ga_2O_3 crystal might depend not only on the segregation coefficient but also the VB growth conditions such as the sintering of raw material with doping SnO_2, the melting temperature and maintaining time, the temperature distribution and growth rate during growth, and other factors.

Table 4 shows the Hall effect measurement result of the carrier density, the mobility, and the resistivity [28] on a representative five samples with dimensions 5 x 5 mm^2 cut from wafers with different Sn concentrations. These five wafers were prepared from an unintentionally doped (UID) crystal ingot and 0.05mol% and 0.1mol% Sn-doped crystal ingots respectively, grown by our VB technique using platinum-rhodium alloy crucibles in the resistance heating furnace with ambient air. The n-type carrier density 5.1 x 10^{16} /cm^3 value of UID wafer No.1 might be mainly due to the residual impurity of several wt.ppm silicon. The carrier density values of wafers Nos.2 and 3 were almost the same as doped Sn concentrations. That the carrier densities values are slightly different from those of Sn concentrations might be related to the residual impurities and/or dopant Sn activation property. On the other hand, in the higher Sn concentration wafer No.4, the carrier density was 1.1 x 10^{18} /cm^3, half the value of doped Sn concentration of 2.2 x 10^{18} atoms/cm^3, and in the highest Sn concentration wafer No.5, the carrier density of 3.6 x 10^{18} /cm^3 was also a smaller value than the Sn concentration of 5.1 x 10^{18} atoms/cm^3, similar to the result with wafer No.4. We could say that the dopant Sn activation seems to have decreased with the Sn concentration increase in the higher concentration region of more than 10^{18} atoms/cm^3. The carrier densities of wafer Nos. 4 and 5 could be increased by studying improved activation treatment because the wafers in Table 4 were not given

any treatment except for the ingot annealing at 1500ºC for 10 hours to release residual stress just after crystal growth. As for the characteristics of the mobility, the measured values decreased with increasing Sn concentration, except for the value with the UID wafer, and as a result, the resistivity values slightly decreased with increasing Sn concentration.

Finally, we can summarize that n-type oxide semiconductor wafer with a carrier density of 3.6 x 10^{18} /cm^3, a mobility of 60.0 cm^2/Vsec and a resistivity of 0.029 Ω-cm could be obtained from a 0.1 mol% Sn-doped crystal.

4. Summary and conclusions

50 mm-diameter Sn-doped β-Ga_2O_3 crystals with growth orientation perpendicular to (001) plane were grown with a 1.0 to 2.0 mm/hour crucible translation rate, in the newly developed resistance heating VB furnace using platinum-rhodium alloy crucibles in ambient air.

As grown crystal ingots after release from the platinum-rhodium alloy crucible showed smooth and shiny surfaces, they were judged as single crystals except for thin surface and periphery portions at the growth end portion. Occasionally, a complete single crystal was also confirmed when grown crystal ingots had very smooth and shiny surfaces throughout conical, body and growth end portions.

In both-side mirror-polished 50 mm-diameter (001) wafers, some weak LAGBs and several small grains were detected by high resolution refraction x-ray topography, however, no imperfections were observed over the whole wafer area by means of crossed polarizer analysis. In the crystallinity evaluation at five positions in the center and at four periphery portions on a 50 mm-diameter (001) wafer, it was found that FWHM values ranged from 8.6 to 46.1 arcsec and dislocation densities ranged from 98 to 2100 /cm^2. We could say that as for the crystallinity on a representative (001) β-Ga_2O_3 wafer, both the FWHM values and the dislocation densities were rather small but widely distributed with no distinctive correlations between them.

In impurity analysis on Sn-doped crystal grown by our VB process, we found that the amount of the dopant Sn concentration in the grown crystal increased with increasing doped Sn concentration in the raw material, however, the concentration change with solidification fraction could not be simply explained in terms of the segregation phenomenon. On the other hand, we found that Sn-doped wafers with concentration ranging from 5 x 10^{17} to 5 x 10^{18} atom/cm^3 could be obtained by Sn-doping ranging from

0.05 to 0.1mol% in the raw material preparation process. We also confirmed that n-type semiconductor wafers with a carrier density of 3.6 x 10^{18} /cm^3, a mobility of 60.0 cm^2/Vsec and a resistivity of 0.029 Ω-cm were obtained from a 0.1mol% Sn-doped crystal.

We concluded in our present study that the 50 mm-diameter Sn-doped single crystal ingots with growth orientation perpendicular to (001) plane were grown with the newly developed resistance heating VB furnace using platinum-rhodium alloy crucibles in ambient air, and that both-side mirror-polished 50 mm-diameter wafers doped with Sn concentration up to 5.1 x 10^{18} atoms/cm^3 were also obtained. The resulting n-type oxide semiconductor wafers might be useful for epitaxial growth substrate.

Acknowledgments

The authors express their gratitude to A. Kajikura from Fujikoshi Machinery Corp. and Dr. T. Taishi from Shinshu University for their helpful and stimulating discussions. Part of this work was supported by “The research and development project for innovation in techniques of energy conservation” of the New Energy and Industrial Technology Development Organization (NEDO), Japan.

References

[1] H. H. Tippins, Optical Absorption and Photoconductivity in the Band Edge of β-Ga_2O_3, Phys. Rev., **140** No.1A (1965) A316-A319.

[2] M. Orita, H. Ohta, M. Hirano, and H. Hosono, Deep-ultraviolet transparent conductive β-Ga_2O_3 thin films, Appl. Phys. Lett., **77** No.25 (2000) 4166-4168.

[3] M. Higashiwaki, K. Sasaki, A. Kuramata, T. Masui, and S. Yamakoshi, Gallium oxide (Ga_2O_3) metal-semiconductor field-effect transistors on single-crystal β-Ga_2O_3 (010) substrates, Appl. Phys. Lett., **100** (2012) 013504.

[4] M. Higashiwaki, K. Sasaki, A. Kuramata, T. Masui, and S. Yamakoshi, Development of gallium oxide power devices, Phys. Status Solidi A, **211** No.1 (2014) 21-26.

[5] T. Oishi, Y. Koga, K. Harada, and M. Kasu, High-mobility β-Ga_2O_3(-201) single crystals grown by edge-defined film-fed growth method and their Schottky barrier diodes with Ni contact, Appl. Phys. Express, **8** (2015) 031101.

[6] E. G. Víllora, S. Arjoca, K. Shimamura, D. Inomata, and K. Aoki, β-Ga_2O_3 and

single-crystal phosphors for high-brightness white LEDs & LDs, and β-Ga_2O_3 potential for next generation of power devices, Proc. of SPIE, **8987** (2014) 89871U.

[7] Michele Baldini, Zbigniew Galazka, and Günter Wagner, Recent progress in the growth of β-Ga_2O_3 for power electronics applications, Materials Science in Semiconductor Processing, **78** (2018) 132-146.

[8] N. Ueda, H. Hosono, R. Waseda, and H. Kawazoe, Synthesis and control of conductivity of ultraviolet transmitting β-Ga_2O_3 single crystals, Appl. Phys. Lett., **70** (26) (1997) 3561-3563.

[9] E. G. Víllora, K. Shimamura, Y. Yoshikawa, K. Aoki and N. Ichinose, Large-size β-Ga_2O_3 single crystals and wafers, J. Cryst. Growth, **270** (2004) 420–426.

[10] E. G. Víllora, K. Shimamura, Y. Yoshikawa, T. Ujiie and K. Aoki, Electrical conductivity and carrier concentration control in β-Ga_2O_3 by Si doping, Appl. Phys. Lett., **92** (2008) 202120.

[11] Y. Tomm, P. Reiche, D. Klimm, and T. Fukuda, Czochralski grown Ga_2O_3 crystals, J. Cryst. Growth, **220** (2000) 510-514

[12] Z. Galazka, R. Uecker, K. Irmscher, M. Albrecht, D. Klimm, M. Pietsch, M. Brützam, R. Bertram, S. Ganschow, and R. Fornari, Czochralski growth and characterization of β-Ga_2O_3 single crystals, Cryst. Res. Technol., **45** No.12 (2010) 1229-1236.

[13] Z. Galazka, K. Irmscher, R. Uecker, R. Bertram, M. Pietsch, A. Kwasniewski, M. Naumann, T. Schulz, R. Schewski, D. Klimm, and M. Bickermann, On the bulk β-Ga_2O_3 single crystals grown by the Czochralski method, J. Cryst. Growth, **404** (2014) 184–191.

[14] H. Aida, K. Nishiguchi, H. Takeda, N. Aota, K. Sunakawa, and Y. Yaguchi, Growth of β-Ga_2O_3 Single Crystals by the Edge-Defined, Film Fed Growth Method, Jpn. J. Appl. Phys., **47** No.11 (2008) 8506–8509.

[15] A. Kuramata, K. Koshi, S. Watanabe, Y. Yamaoka, T. Masui and S. Yamakoshi, High-quality β-Ga_2O_3 single crystals grown by edge-defined film-fed growth, Jpn. Journal of Applied Physics **55**, (2016) 1202A2.

[16] E. G. Víllora, Y. Morioka, T. Atou, T. Sugawara, M. Kikuchi, and T. Fukuda, Infrared Reflectance and Electrical Conductivity of β-Ga_2O_3, Phys. Stat. Sol. (a), **193** No.1 (2002) 187-195.

[17] M. Zinkevich and F. Aldinger, Thermodynamic Assessment of the Gallium-Oxygen System, J. Am. Ceram. Soc., **87** [4] (2004) 683–691.

[18] D. Klimm, S. Ganschow, D. Schulz, R. Bertram, R. Uecker, P. Reiche, and R. Fornari,

Growth of oxide compounds under dynamic atmosphere composition, J. Cryst. Growth, **311** (2009) 534–536.

[19] K. Hoshikawa, H. Nakanishi, H. Kohda, and M. Sasaura, LIQUID ENCAPSULATED, VERTICAL BRIDGMAN GROWTH OF LARGE DIAMETER, LOW DISLOCATION DENSITY, SEMI-INSULATING GaAs, J. Cryst. Growth, **94** (1989) 643-650.

[20] S. Uda, H. Inaba, J. Harada, K. Hoshikawa, Growth of langasite via Bridgman technique along [0001], [2110] and [0111] for piezoelectric applications, Journal of Crystal Growth, **271** (2004) 229-237.

[21] C. Miyagawa, T. Kobayashi, T. Taishi, K. Hoshikawa, Development of the Vertical Bridgman Technique for 6-inch Diameter c-axis Sapphire Growth Supported by Numerical Simulation, Journal of Crystal Growth, **402** (2014) 83-89.

[22] K. Hoshikawa, E. Ohba, T. Kobayashi, J. Yanagisawa, C. Miyagawa, and Y. Nakamura, Growth of β-Ga_2O_3 single crystals using vertical Bridgman method in ambient air, J. Cryst. Growth **447** (2016) 36-41.

[23] E. Ohba, T. Kobayashi, M. Kado, and K. Hoshikwa, Defect characterization of β-Ga_2O_3 single crystals grown by vertical Bridgman method, Jpn. J. Appl. Phys., **55** (2016) 1202BF.

[24] K. Hoshikawa, T. Kobayashi, Y. Matsuki, E. Ohba, and T. Kobayashi, 2-inch Diameter (100) β-Ga_2O_3 Crystal Growth by the Vertical Bridgman Technique in a Resistance Heating Furnace in Ambient Air, Journal of Crystal Growth, **545** (2020) 125724.

[25] M. Higashiwaki, K. Konishi, K. Sasaki, K. Goto, K. Nomura, Q. T. Thieu, R. Togashi, H. Murakami, Y. Kumagai, B. Monemar, A. Koukitu, A. Kuramata, and S. Yamakoshi, Temperature-dependent capacitance–voltage and current–voltage characteristics of Pt/Ga_2O_3 (001) Schottky barrier diodes fabricated on n^-–Ga_2O_3 drift layers grown by halide vapor phase epitaxy, APPLIED PHYSICS LETTERS **108**, (2016) 133503.

[26] K. Sasaki, D. Wakimoto, Q. T. Thieu, Y. Koishikawa, A. Kuramata, M. Higashiwaki, and S. Yamakoshi, First Demonstration of Ga_2O_3 Trench MOS-Type Schottky Barrier Diodes, IEEE ELECTRON DEVICE LETTERS, VOL. 38, NO. 6, (2017) 783.

[27] T. Taishi, X. Huang, I. Yonenaga, K. Hoshikawa, Dislocation-free Czochralski Si crystal growth without a thin neck: dislocation behavior due to incomplete seeding, Journal of Crystal Growth, **258** (2003) 58–64.

[28] N. Suzuki, S. Ohira, M. Tanaka, T. Sugawara, K. Nakajima and T. Shishido, Fabrication and characterization of transparent conductive Sn-doped β-Ga_2O_3 wafer

single crystal, Phys. Stat. Sol. (c)**4**, No. 7, (2007) 2310-2313.

[29] Z. Galazka, K. Irmscher, R. Schewski, I. M. Hanke, M. Pietsch, S. Ganschow, A. Dittar, A. Fiedler, T. Schroeder and M. Bickermann, Czochralski-grown bulk β-Ga_2O_3 crystals doped with mono-, di-, tri, and tetravalent ions, Journal of Crystal Growth, **529** (2020) 125297.

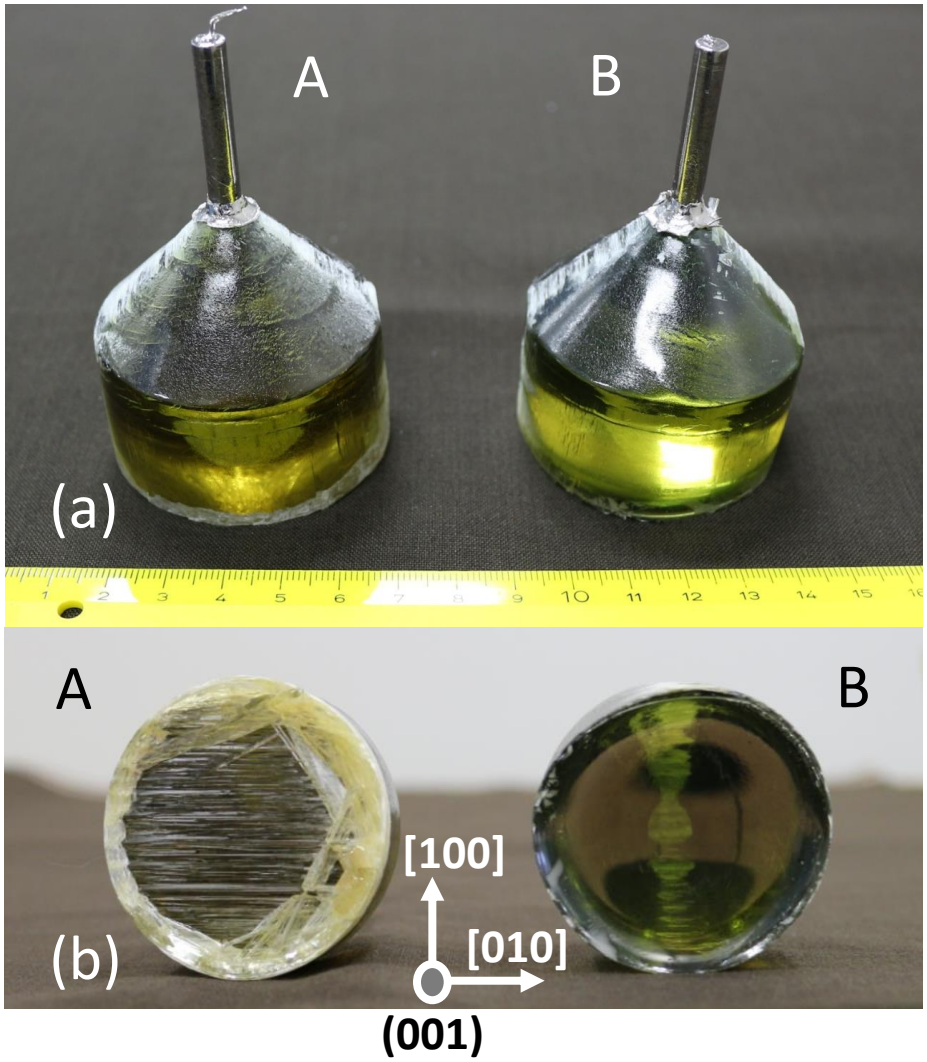

Fig. 1 Photographs of as-grown 50mm-diameter Sn-doped β-Ga_2O_3 crystal ingots with growth orientation perpendicular to (001) plane.

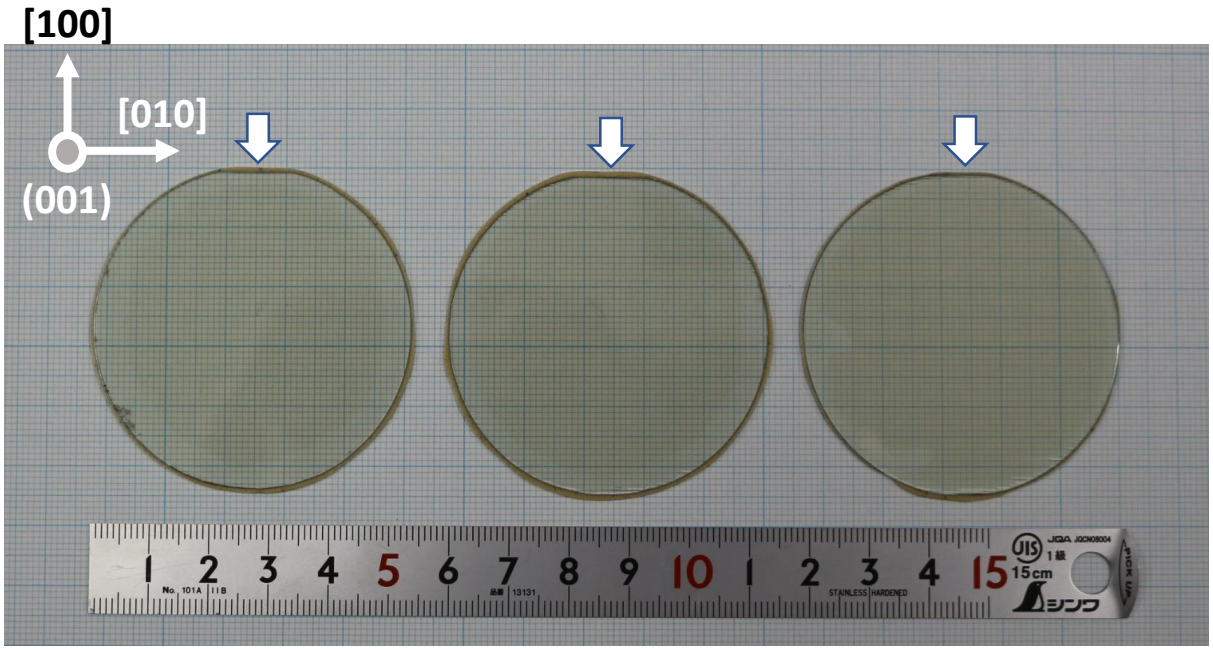

Fig. 2 Photograph of 50mm-diameter both-side-mirror polished (001) β-Ga_2O_3 wafers with about 0.7mm thickness.

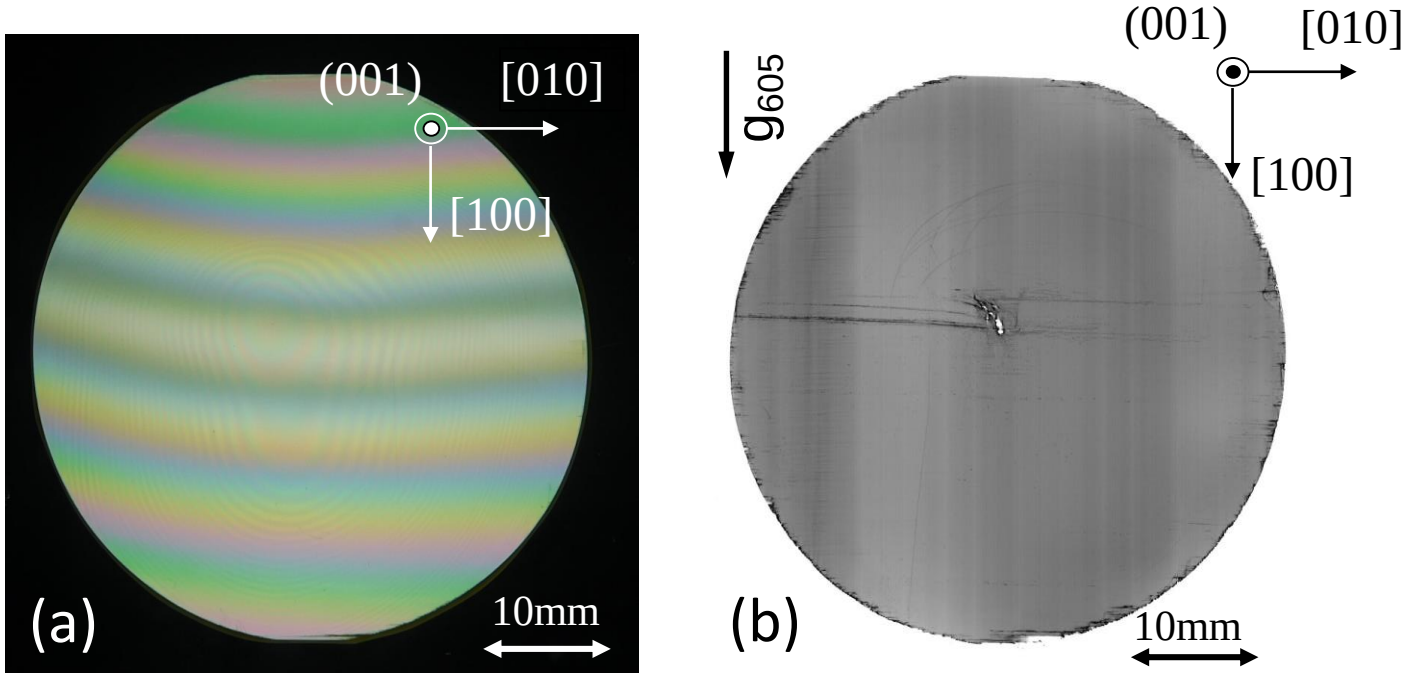

Fig. 3 Crossed polarizer observation image (a) and refraction x-ray topographic image (b) of 50mm-diameter (001) wafers cut from ingot A shown in Fig. 1.

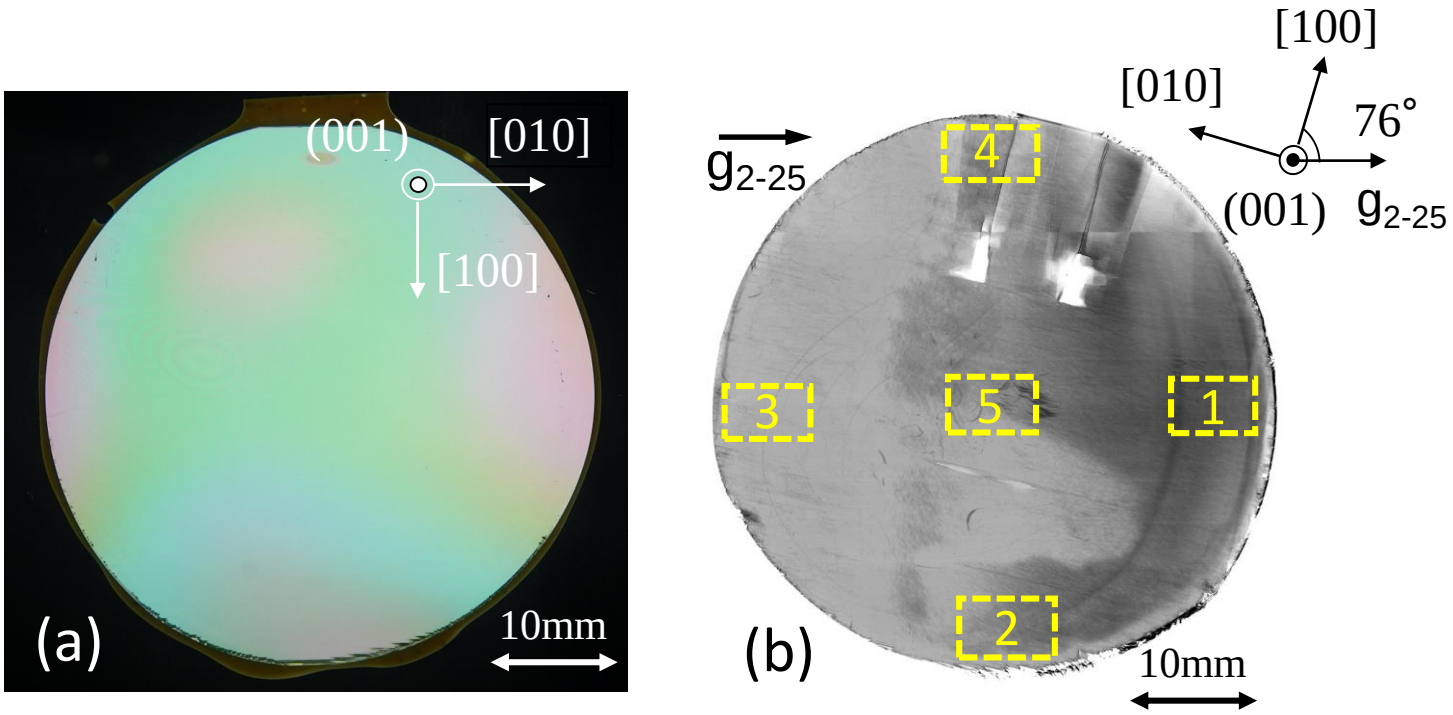

Fig. 4 Crossed polarizer observation image (a) and refraction x-ray topographic image (b) of 50mm-diameter (001) wafers cut from ingot B shown in Fig. 1.

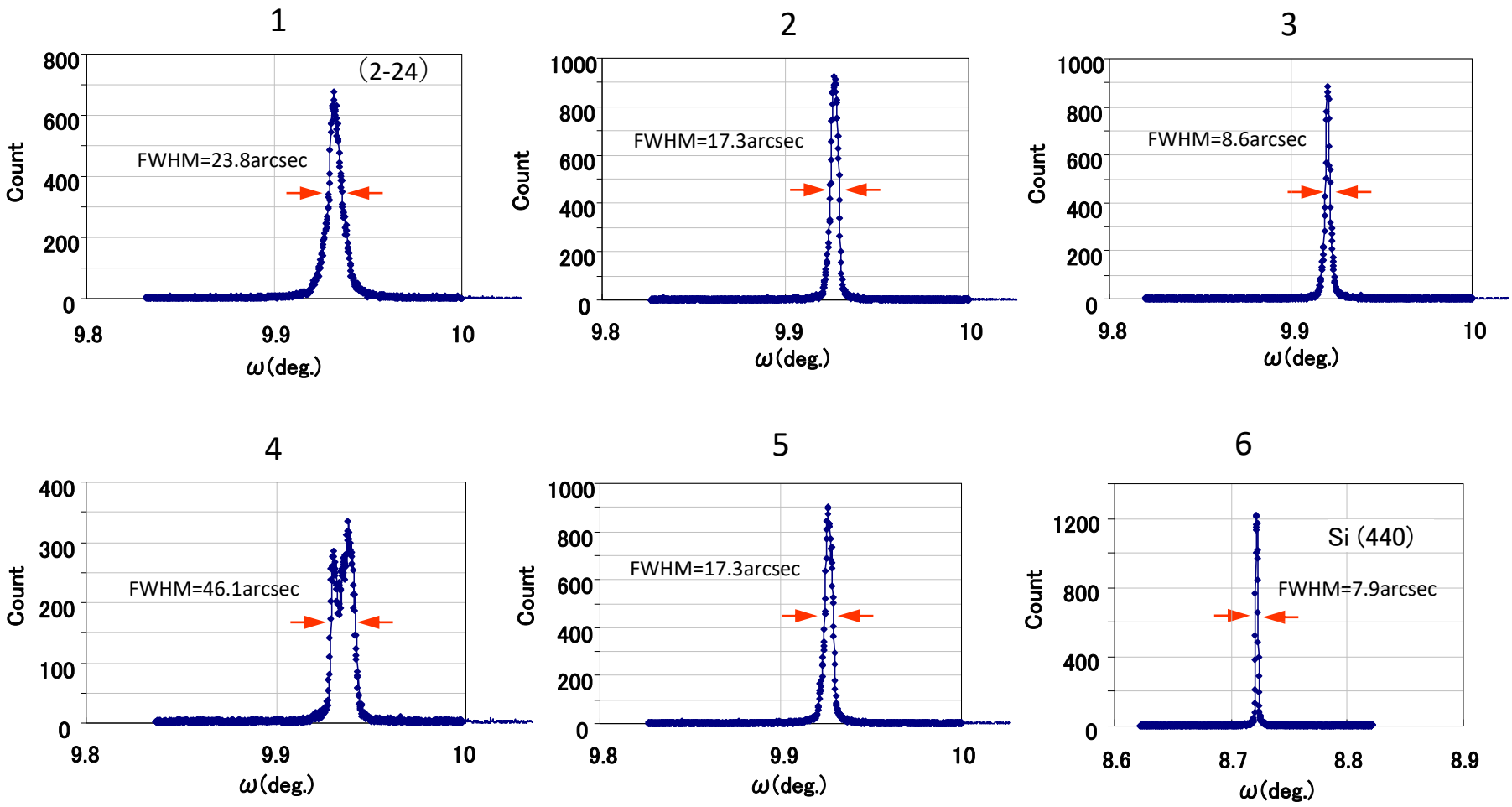

Fig. 5 X-ray rocking curves on the wafer shown in Fig. 4(b). Curves 1, 2, 3, 4 and 5 correspond to the numbered portions indicated with rectangles in the figure.

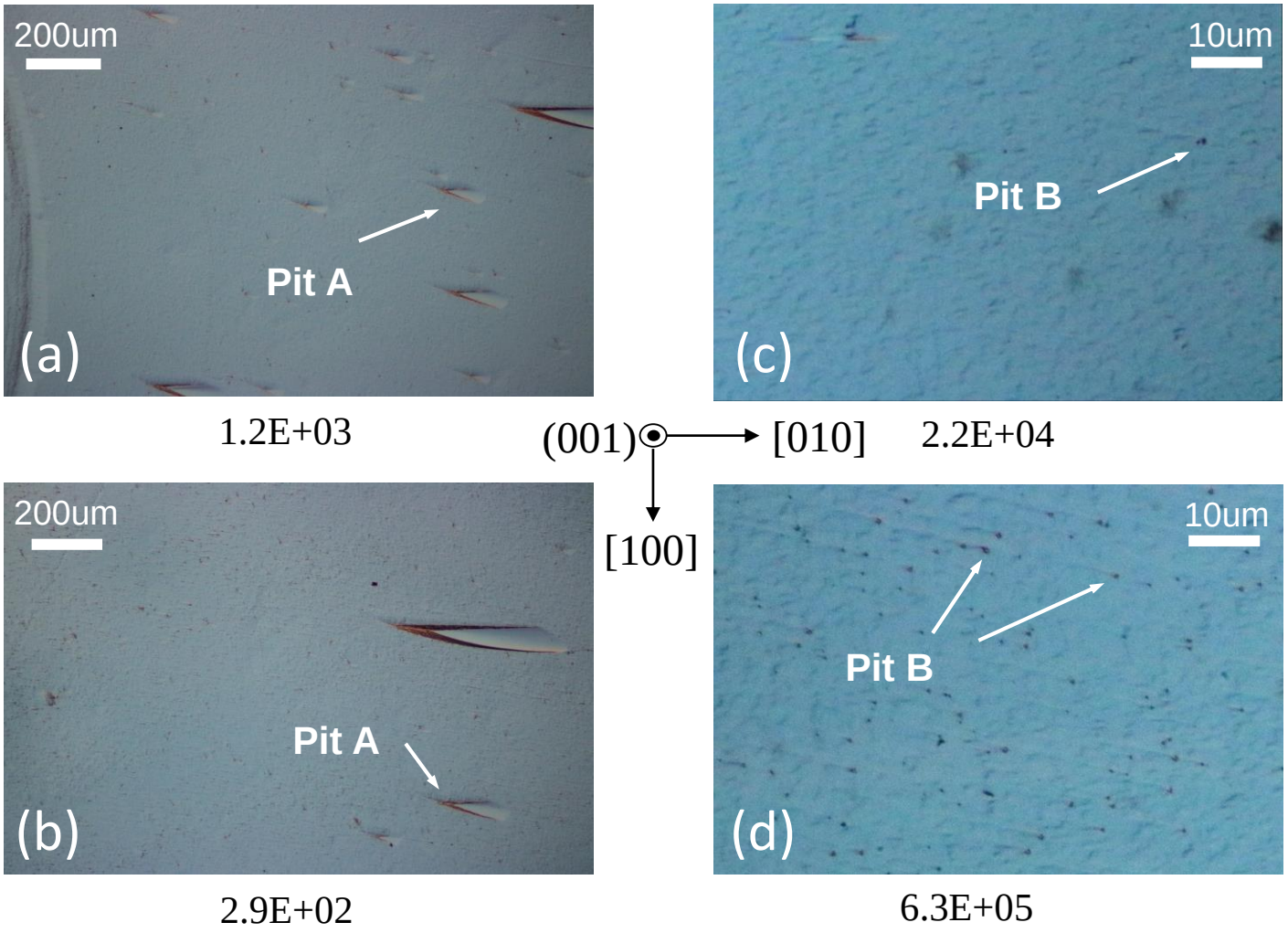

Fig. 6 Photographs of two kinds of etch pits A and B revealed by KOH etching after the x-ray topography analysis shown in Fig. 4(b).

Table 1 Distributing characteristics of FWHM values and densities of etch pits A and B for the five portions on the wafer indicated by rectangles in Fig. 4(b).

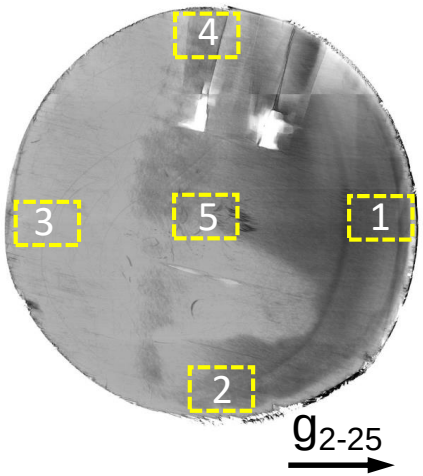

Position	FWHM arcsec	Etch pit density cm^{-2}	
		Pit A	Pit B
1	23.8	$2.1x10^3$	$2.0x10^5$
2	17.3	$9.8x10^1$	$1.1x10^6$
3	8.6	$2.9x10^2$	$6.3x10^5$
4	46.1	$9.8x10^2$	$2.6x10^5$
5	17.3	$1.2x10^3$	$2.2x10^4$

Table 2 Result of GDMS impurity analysis on two crystals A and B with g=0.2.

Element	Crystal A (0.05mol% doping) Analyzed value [wt.ppm]	Crystal B (0.1mol% doping) Analyzed value [wt.ppm]
Na	<0.02	0.04
Al	0.34	1.7
Si	2.6	1.4
Ca	0.38	0.71
Fe	1.2	1.3
Zr	1.3	0.48
Sn	14	83
Rh	28	38
Pt	0.01	0.02
Ir	<0.01	<0.01

Table 3 Solidification fraction g vs Sn concentration in crystal grown with 0.1 mol% Sn-doping.

Solidification fraction of sample g	Sn concentration [wt. ppm]
0.10	170
0.20	83
0.40	89
0.60	70
0.85	86
0.95	82

Table 4 Hall effect measurement result of carrier density, mobility and resistivity vs Sn concentration on representative five samples.

Wafer No.	Sn concentration [atoms/cm^3]	Carrier density [/cm^3]	Mobility [cm^2/V sec]	Resistivity [Ω-cm]
1	UID	$5.1x10^{16}$	90.5	1.35
2	$4.2x10^{17}$	$4.7x10^{17}$	111	0.119
3	$6.9x10^{17}$	$7.1x10^{17}$	89.6	0.099
4	$2.2x10^{18}$	$1.1x10^{18}$	84.7	0.066
5	$5.1x10^{18}$	$3.6x10^{18}$	60.0	0.029